Research article

Marina Garcia-Pardo, Eva Nieto-Pinero, Amanda K. Petford-Long, Rosalia Serna* and Johann Toudert*

Active analog tuning of the phase of light in the visible regime by bismuth-based metamaterials

https://doi.org/10.1515/nanoph-2019-0502
Received December 4, 2019; revised January 17, 2020; accepted February 4, 2020

Abstract: The active and analog tuning of the phase of light by metamaterials is needed to boost the switching performance of photonic devices. However, demonstrations of this type of tuning in the pivotal visible spectral region are still scarce. Herein, we report the active analog tuning of the phase of visible light reflected by a bismuth (Bi)-based metamaterial, enabled by a reversible solid-liquid transition. This metamaterial, fabricated by following a lithography-free approach, consists of two-dimensional assemblies of polydisperse plasmonic Bi nanostructures embedded in a refractory and transparent aluminum oxide matrix. The analog tuning of the phase is achieved by the controlled heating of the metamaterial to melt a fraction of the nanostructures. A maximum tuning of 320° (1.8 π) is observed upon the complete melting of the nanostructures at 230°C. This tuning is reversible by cooling to 25°C. In addition, it presents a wide hysteretic character due to liquid Bi undercooling. This enables the phase achieved by this analog approach to remain stable over a broad temperature range upon cooling and until re-solidification occurs around 100°C. Therefore, Bi-based metamaterials are endowed with analog optical memory capabilities, which are appealing for a wide range of applications, including optical data storage with enhanced information density or bistable photonic switching with a tunable "on" state.

***Corresponding authors: Rosalia Serna and Johann Toudert,** Laser Processing Group, Instituto de Óptica, IO, CSIC, Madrid, Spain, e-mail: rosalia.serna@csic.es (R. Serna); johann.toudert@gmail.com (J. Toudert). https://orcid.org/0000-0002-1609-1934 (J. Toudert)
Marina Garcia-Pardo and Eva Nieto-Pinero: Laser Processing Group, Instituto de Óptica, IO, CSIC, Madrid, Spain
Amanda K. Petford-Long: Materials Science Division, Argonne National Laboratory, Argonne, IL, USA; and Materials Science and Engineering Dept, Northwestern Univ, Evanston, IL, USA

Keywords: phase change material; metamaterial; bismuth; phase; visible.

1 Introduction

Metamaterials that enable the active tuning of the amplitude and phase of light are needed to boost the performance of photonic devices, such as optical modulators, reconfigurable antennas, polarization controllers, displays and optical data storage media [1]. In this context, phase change metamaterials (PCMs) based on compounds, such as VO_2 or $GeSb_xTe_y$ (GSTs), have been thoroughly considered, because their optical properties can be tuned reversibly via externally triggered phase transitions [2–19]. The optical properties of VO_2 change upon its monoclinic/tetragonal transition. The tetragonal phase forms upon heating above 65°C, and the monoclinic phase recovers upon cooling below this temperature [2–7]. This volatile characteristic is an asset for optical modulators, polarization controllers or reconfigurable antennas. However, for other applications such as optical data storage, GSTs are preferred because of their non-volatile amorphous/crystalline transition. In contrast with VO_2, the crystalline phase that is formed upon heating above 250°C remains upon cooling [8–19]. However, returning to the original amorphous phase requires energetic processes, such as melt-quenching near 600°C or irradiation with electrons or light pulses [8, 10, 12, 15, 16, 18].

Interestingly, although tuning based on a phase transition conveys a binary picture involving an "off" and an "on" state, the multilevel and even analog tuning of the optical properties of PCMs have been recently reported [4, 6, 7, 13, 14, 16–18]. This paves the way for the creation of photonic devices with outstanding features, such as colors that can be tuned actively and in an analog manner, or optical data storage with enhanced information density. The fine tuning reported in these works has been made possible by triggering the phase transition of a controlled volume fraction of the material, thus achieving

a controlled proportion of both phases. This, in turn, enables the analog tuning of the amplitude of light transmitted by Mie and anapole resonant GST metasurfaces [17], and of the phase of light reflected by Au/VO_2/Au gap plasmon metasurfaces [6]. Such tuning has been demonstrated in the mid- and near-infrared (IR), respectively. In fact, most of the reports showing PCMs with actively tunable optical properties have focused on these spectral regions, wherein the optical response of VO_2 and GSTs is the most strongly affected by their crystallinity [2–4, 6, 8, 9, 11–15, 17]. Meanwhile, demonstrations of PCMs that enable an active analog tuning of the amplitude and phase of light in the pivotal visible and ultraviolet (UV) regions remain scarce. Only recently have some reports showed active multilevel or analog color tuning with PCMs based on VO_2 and GST nanolayers [7, 16, 18].

As an alternative to VO_2 and GSTs, in previous works, we have proposed the use of bismuth (Bi) nanostructures as the active building blocks of PCMs, thus enabling the tuning of UV and visible light [20–22]. Bi is an outstanding optical material that presents UV-visible plasmonic properties induced by giant interband transitions in the solid state [21, 23–26]. Upon heating above 270°C, it undergoes a solid/liquid transition that rubs out these interband transitions, so that the liquid Bi behaves as a lossy Drude metal [27]. The solid/liquid transition markedly changes the spectrum of the Bi dielectric function in the UV and visible light, as shown in Figure 1A. This change induces a shift in the plasmon resonances of the Bi nanostructures, which then translates into a significant change in the UV-visible optical properties of the PCM. When the nanostructures melt, their size, shape and organization remain unchanged. This is because in the considered PCMs, the Bi nanostructures are embedded in a refractory matrix, which acts as a solid mold. This matrix also enables the nanostructures to return to their initial solid state upon decreasing the temperature [20, 28]. On the basis of such behavior, in a previous work, we reported the applicability of Bi-based PCMs for the high-contrast binary switching of the amplitude of light [22]. However, the potential of Bi-based PCMs for analog tuning and phase tuning remains unexplored in the literature.

Herein, we demonstrate the active analog tuning of the phase of visible light reflected by a Bi-based PCM. Such tuning is achieved by the controlled heating of the PCM at a selected temperature to melt a fraction of the embedded Bi nanostructures. A maximum tuning of the phase of light of 320° (1.8 π) is observed upon the complete melting of the nanostructures at 230°C. The tuning is fully reversible by cooling to 25°C, yet with a wide hysteretic response due to Bi undercooling. This endows the PCM with analog

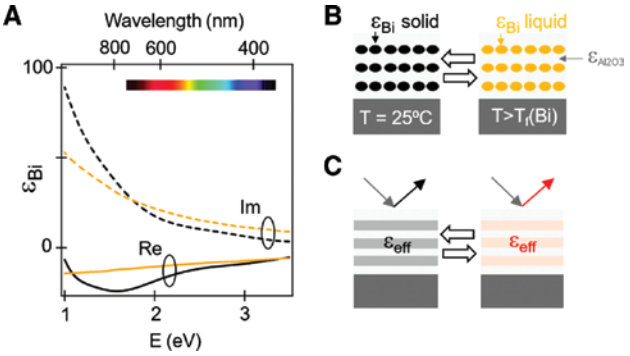

Figure 1: The working principle of the Bi-based PCM. (A) The spectra of the real and imaginary part of the dielectric function ε_{Bi} of solid Bi (black lines, from [25]) and liquid Bi (orange lines, from [27]). (B) Simplified cross-section drawing of the PCM design consisting of a multilayer stack alternating composite Bi:Al_2O_3 nanolayers with spacer layers made of Al_2O_3. Each composite nanolayer consists of a 2D assembly of Bi nanostructures embedded in Al_2O_3. Upon increasing temperature above the Bi melting point, the nanostructures melt and the dielectric function of each nanostructure changes from that of solid Bi to that of liquid Bi, represented in (A). (C) Therefore, upon melting the Bi nanostructures, the effective dielectric function ε_{eff} of the composite nanolayers changes along with the optical reflection properties of the PCM. Note that the dielectric function ε_{Al2O3} of Al_2O_3 does not change significantly over the range of temperatures considered.

optical memory capabilities, which have interesting applications in optical data storage with enhanced information density or in bistable photonic switching with a tunable "on" state, among others.

The PCM was designed according to the simplified cross-section drawing in Figure 1B. It consists of a multilayer stack of alternating Bi:Al_2O_3 composite nanolayers and Al_2O_3 spacer layers, which are deposited on a reflective substrate (Si). Each composite nanolayer consists of a two-dimensional (2D) assembly of Bi nanostructures embedded in Al_2O_3. For this experiment, we have selected Al_2O_3 as the embedding medium because of its excellent thermal stability and transparency; however, other refractory and transparent materials could be used. As shown in Figure 1C, as Bi melts, the effective dielectric function of the composite nanolayers changes significantly. This results in a change in the optical reflection properties of the whole PCM, which are driven by the interplay between plasmon resonances in the composite nanolayers and optical interference in the whole multilayer stack [29]. Due to this interplay, the reflected amplitude and phase spectra of the PCM are not simple replicas of its plasmon resonances. In contrast, these spectra may present complex features that can, for instance, be detuned from such resonances

while still being sensitive to them [29]. Therefore, remarkable spectral features can be achieved for the PCM upon specific "man-made" design. Such design requires combining a suitable effective dielectric function of the composite nanolayers with a suitable vertical organization of the layers, in order to achieve the targeted interference properties and reflected amplitude and phase spectra. At such an aim, the nanostructure of the composite nanolayers and the layer thicknesses must be controlled accurately, and the number of layers must be suitably chosen. Such control can be achieved through fabrication processes that do not require costly or low-throughput lithography techniques. Therefore, materials that are built following these design rules for the control of interference properties and reflected amplitude and phase spectra are often named "lithography-free metamaterials" [30, 31]. When based on Bi, such metamaterials are ideal for narrowband color filtering and ultrabroadband near perfect absorption [31]. The lithography-free PCMs considered in this work are intentionally designed with the aim of harnessing the interplay between plasmon resonances and optical interference, in order to achieve a broad tuning of the phase of reflected light in the visible.

2 Results and discussion

2.1 PCM structure and temperature-dependent optical properties

Bi-based PCMs were produced by pulsed laser deposition, a fully lithography-free material fabrication technique (Methods section, PCM fabrication). A cross-section transmission electron microscopy image of one of the fabricated Bi-based PCMs is shown in Figure 2A. The light-contrast areas in the image correspond to the Al_2O_3 spacer layers. The Al_2O_3 is amorphous. The five dark-contrast areas correspond to the Bi:Al_2O_3 composite nanolayers, which present an approximate thickness of 6 nm (Methods section, PCM structure). Each of these nanolayers consists of a 2D assembly of Bi nanostructures embedded in Al_2O_3. The nanostructures show oblate ellipsoidal

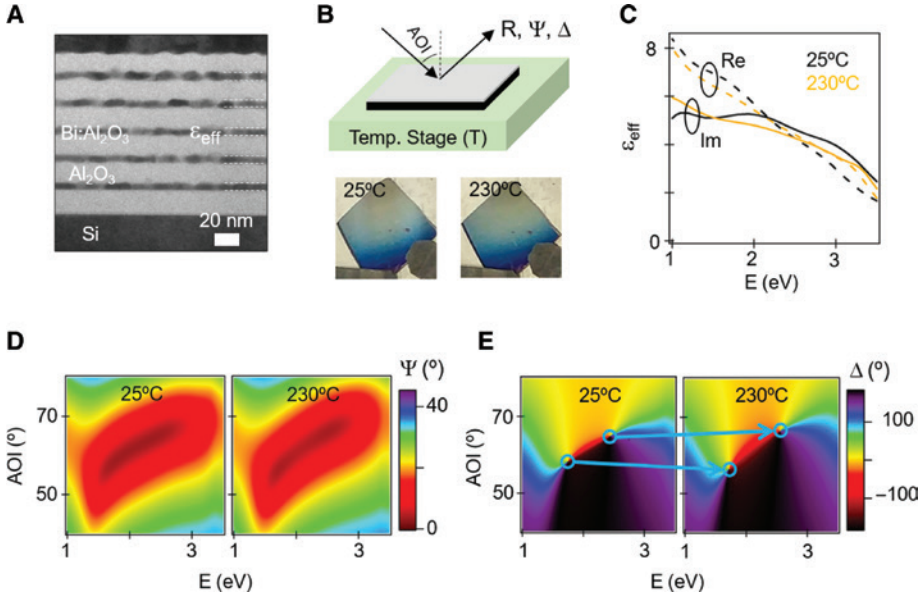

Figure 2: The structure- and temperature-dependent optical properties of the fabricated Bi-based PCM.
(A) The cross-section image of the fabricated PCM obtained by transmission electron microscopy. The five Bi:Al_2O_3 composite nanolayers, which appear as five dark-contrast areas, consist of polydisperse Bi nanostructures embedded in Al_2O_3. (B) The configuration used for temperature-dependent optical measurements and macroscopic images of the PCM taken at 25°C and 230°C. (C) The spectra of the effective dielectric function of the composite nanolayers at 25°C and 230°C. In contrast with Figure 1A, which represents the dielectric function of each Bi nanostructure, the effective dielectric function shown here stands for each Bi:Al_2O_3 composite nanolayer. (D) The interpolated maps of the ellipsometric amplitude coefficient, ψ, of the PCM as a function of photon energy E and angle of incidence AOI at 25°C and 230°C. (E) The corresponding maps of the ellipsometric phase coefficient, Δ. The maps show two singularities (marked with circles) that are displaced upon increasing temperature (arrows), as a result of the Bi nanostructures melting. Near these singularities, the phase of light reflected by the PCM varies strongly with the temperature.

shapes with a broad polydisperse size and shape distribution (Methods section, Size and shape distribution). This PCM was placed on the temperature-controlled stage of a spectroscopic ellipsometer, as shown in Figure 2B, to measure its optical properties as a function of temperature T (25°C–240°C), angle of incidence AOI (20°–75°) and photon energy E (1.0–3.5 eV) covering the visible and part of the near-IR wavelength range (350–1240 nm). The measurements were first carried out under static conditions, i.e. after stabilizing T at a fixed value (Methods section, Temperature-dependent optical properties).

Figure 2C shows the spectra of the effective dielectric function of the Bi:Al_2O_3 composite nanolayers at 25°C and 230°C as determined by spectroscopic ellipsometry (Methods section, Temperature-dependent optical properties). These spectra present a featureless spectral shape resulting from the broad size and shape distribution of the Bi nanostructures, inducing a strong inhomogeneous broadening that combines with the already strong intrinsic broadening of the Bi plasmon resonances [23]. The clear contrast seen between the spectra at 25°C and 230°C results from the different states of the Bi nanostructures at T = 25°C and 230°C (solid and liquid, respectively). The Bi nanostructures are fully melted at 230°C, i.e. 40°C below the bulk Bi melting point. This agrees with the size-dependence of the Bi solid/liquid transition reported in previous works [32].

Although it does not seemingly affect the visual aspect of the PCM surface (see image Figure 2B), the melting of the Bi nanostructures clearly changes the ellipsometric response of the PCM in a way that is explained below. The ellipsometry response of the PCM is shown in Figure 2D and E. Figure 2D displays the interpolated maps of the ellipsometric amplitude coefficient ψ vs. E and AOI, at T = 25°C and 230°C. Similar features are seen at both temperatures, in agreement with the seemingly absent change in visual aspect, with very small ψ values in a broad range of E and for AOIs between 55° and 65°. The interpolated maps of the ellipsometric phase coefficient Δ shown in Figure 2E correlate with those of ψ. However, the maps of Δ display two singularities located at (i: 2.45 eV, 64.5°) and (ii: 1.75 eV, 58.5°) when T = 25°C. Within the energy range of these singularities, strong vortex-like variations of Δ can be found in the E–AOI plane, as large as 360° (phase change of 2 π). The singularities are markedly displaced when T is increased to 230°C: they are at (i: 2.55 eV, 66.5°) and at (ii: 1.72 eV, 56.5°). Thus, at E and AOI values close to these singularities, the phase of light reflected by the PCM varies strongly when the temperature is increased and the Bi nanostructures melt. This effect is closely related to the concept of topological optical darkness [33–36], which is contiguous to the field of metamaterials. Herein, we take advantage of this effect to demonstrate a broad tuning of the phase of light by temperature control.

2.2 Broad phase tuning by temperature control

To analyze and quantify this broad tuning, we studied the optical properties of the PCM at several temperatures from 25°C to 230°C, for an AOI of 64.5°. This AOI was chosen to approach the singularity (i) predicted by the interpolated Δ map of Figure 2E. The measurements were done in static conditions at fixed T's as previously (Methods section, Temperature-dependent optical properties). Figure 3A displays the measured ψ spectra, which all show a clear minimum when E is close to 2.35 eV. Such a minimum is due to the near-cancelation of the p-polarized reflectance (R_p) of the PCM when E is close to 2.35 eV, as seen in Figure 3B. This near-cancelation is the result

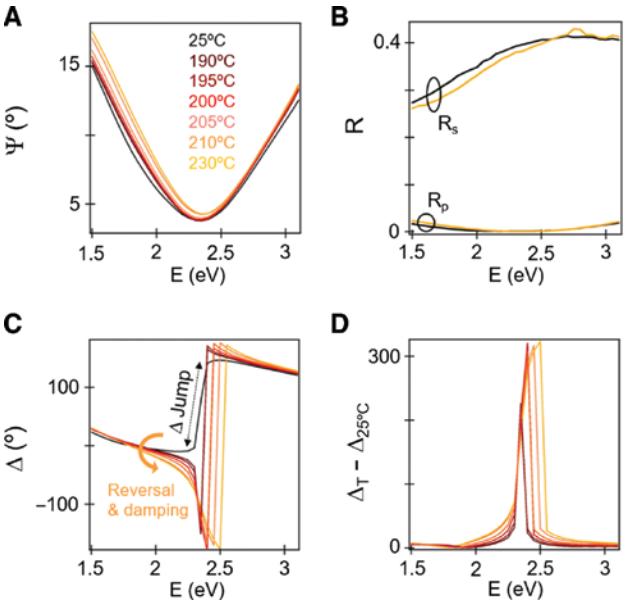

Figure 3: The broad and analog tuning of the phase of visible p-polarized light reflected by the Bi-based PCM.
(A) The ψ spectra of the PCM for an AOI of 64.5° measured at different temperatures between 25°C and 230°C. (B) The corresponding p-polarized and s-polarized reflectance spectra (measured at 25°C and at 230°C only). Near 2.35 eV, R_p is nearly cancelled (R_p = 0.17% and 0.14% at 25°C and 230°C, respectively) (C) The corresponding Δ spectra, which show a jump near 2.35 eV. The initial jump at room temperature is marked by a double arrow. Upon increasing the temperature, the jump reverses (and so does the sign of Δ) and then dampens. This yields a continuous variation of Δ with temperature, which is due to the progressive melting of the Bi nanostructures. (D) The corresponding Δ variation with respect to its value at 25°C, showing a maximum of 320° at 230°C, when the Bi nanostructures are fully melted. The Δ variation with temperature results exclusively from a variation in the phase of the p-polarized reflected light.

of destructive interference between the directly reflected wave and multiply reflected waves escaping from the PCM. This mechanism involves the interplay between the localized plasmon resonances in the composite Bi:Al_2O_3 nanolayers and the interfering waves reflected on the internal interfaces of the layered metamaterial structure [29]. To achieve the near-cancelation of R_p by destructive interference of the reflected waves, sufficient propagation is required for light inside the PCM. Therefore, a minimum thickness of PCM with several interfaces is needed. To fulfil these requirements while simultaneously enabling a strong Bi-light interaction, we deliberately chose to grow several composite Bi:Al_2O_3 nanolayers separated by the Al_2O_3 spacer layers (see Methods section).

The near-cancelation of R_p implies that the phase δ_p of the p-polarized reflected light undergoes a sharp jump in the spectrum for photon energies near 2.35 eV [37–39]. In contrast, the phase δ_S of the s-polarized reflected light is nearly photon energy-independent. Therefore, the spectrum of $\Delta = \delta_P - \delta_S$ shown in Figure 3C displays a sharp jump when E is close to 2.35 eV, which is due to the jump in δ_P. As seen in Figure 3C, upon increasing T, the Δ jump reverses (and so does the sign of Δ) and then dampens. At photon energies close to the jump, Δ is very sensitive to T, and the variation of Δ with T comes exclusively from that of δ_P. Therefore, our results show that, at photon energies close to 2.35 eV, the phase of p-polarized light reflected by the PCM can be broadly tuned by controlling the temperature.

Notably, as this broad tuning is based on the near cancelation of R_p, the design considered here is not ideal for applications requiring a high reflectance. The same is true for the gap-plasmon metamaterials that are used for optical phase tuning, which also display a low reflectance [6]. However, our design has the potential to present a high optical transmittance as no thick metal back reflector is needed. Indeed, upon proper tailoring of the composite nanolayers and with the metamaterial being backed by a high index transparent substrate, strong optical phase tuning could be achieved with almost no optical absorption [29]. This is appealing for the design of active optical devices making an efficient use of optical power, and in which readout of low-level reflected signals is needed (e.g. data encryption or photonic switches for security).

The tuning range of Δ (equivalent to that of δ_p) is quantified in Figure 3D with respect to the initial Δ value at 25°C. Upon increasing T to 230°C, a variation in Δ that is larger than 180° (π) is observed at photon energies between 2.35 eV and 2.5 eV. This spectral window, which corresponds to wavelengths between 527 nm and 496 nm, is broad enough to be accessible with cost-effective thermally-tunable green laser diodes. The maximum Δ variation reached is 320° (1.8 π), and this variation occurs upon a T variation of a few °C between 210°C and 230°C. The sensitivity of Δ to T is less marked in a range of photon energies detuned from the Δ jump. For convenience, we focus on this lower sensitivity range to provide evidence for the analog character of the phase tuning. This character is, for instance, confirmed at E = 2.3 eV, where Δ decreases continuously upon increasing T, yet with a saturation when T approaches 230°C.

2.3 Analog tuning, reversibility and hysteretic behavior

We propose that this analog phase tuning is made possible by the fact that the Bi nanostructures do not all melt at a single temperature. There are two possible reasons for this. (i) The Bi melting point is size-dependent [32]. Thus, as the Bi nanostructures are polydisperse in size, heating the PCM to T < 230°C melts only a fraction of them. (ii) Melting starts from the nanostructure surface. This effect, which we observed for the Bi nanostructures, occurs in a similar way as in Ga nanostructures, which are comparable with Bi nanostructures in terms of thermodynamic and plasmonic properties [40–43]. According to a surface-melting model, the melting rate is driven by the surface/volume ratio of the nanostructure; hence, smaller nanostructures are easier to melt than larger ones.

Thus, considering both scenarios (i) and (ii), as shown in Figure 4A, the proportions of solid and liquid Bi in the PCM are set by the heating temperature. This enables the analog tuning of the optical properties of the PCM and, therefore, of the phase δ_p of p-polarized reflected light represented here by the ellipsometric phase coefficient Δ.

To ascertain the analog character of the phase tuning, and to show its reversibility and hysteretic properties, we finally measured Δ at a single value of E (2.3 eV) and AOI (64.5°) as a function of T under dynamic conditions (Methods section, Temperature-dependent optical properties). In this case, Δ was continuously monitored while heating from room temperature $T_1 = 25$°C to a selected maximum value $T_2 < 230$°C and then while cooling down to room temperature T_1. The left panel of Figure 4B displays the $\Delta = f(T)$ curve recorded for $T_2 = 195$°C. Upon heating, Δ starts decreasing when T is ~185°C, i.e. when the smallest Bi nanostructures fully melt. By increasing T further to a selected value, a proportion of the Bi melts so that Δ is decreased to a finely tuned value. This shows the fully analog character of the phase tuning. After reaching T_2, cooling down leaves Δ almost unchanged near a value Δ_{23} until T reaches T_3 ~90°C. We also carried out control experiments to check that this effect is not due

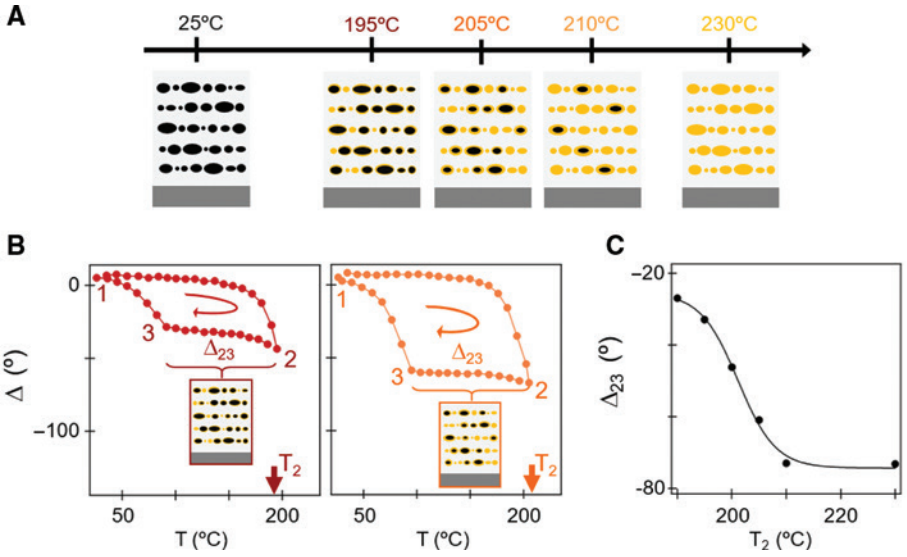

Figure 4: The analog, reversible and hysteretic character of the phase tuning.
(A) The proposed microscopic origin for the analog character of the phase tuning. The Bi melting point is size-dependent and size-dependent surface melting occurs; hence, a controlled fraction of the polydisperse Bi nanostructures can be melted by heating the PCM to a given temperature. At 25°C, 100% of the nanostructures are solid (black). At 230°C, 100% are liquid (orange). (B) The $\Delta = f(T)$ curves for the PCM recorded continuously when heating to a temperature T_2 and then cooling to 25°C. Left panel: $T_2 = 195$°C; Right panel: $T_2 = 205$°C. These curves show the reversibility and hysteretic character of the phase tuning. The Bi melted at point 2 remains in a liquid state when decreasing the temperature to point 3 (undercooling). This leaves Δ almost unchanged near a value Δ_{23} over a broad temperature range (~100°C). Δ_{23} is defined as the Δ value midway from T_2 to T_3 on the hysteresis. (C) Such a stable value of Δ_{23} can be tuned in an analog manner by controlling the fraction of melted Bi, i.e. by properly choosing T_2. All the data in this figure were recorded for E = 2.3 eV and AOI = 64.5°.

to thermal inertia. In these experiments, cooling was stopped to stabilize T between T_2 and T_3. In such static conditions, which were maintained during more than 1 h, Δ remained unchanged near Δ_{23}. Therefore, we attribute the persistence of the Δ value to undercooling, which has been shown to occur for Bi nanostructures [28]. Finally, upon further cooling to T_1, Δ returns to its initial value. The $\Delta = f(T)$ curve thus demonstrates the reversibility of the phase tuning, together with its wide hysteretic behavior ($\delta T \sim 100$°C).

Furthermore, we found it particularly interesting that the Δ_{23} value (and thus the height of the hysteresis) is set by the maximum heating temperature T_2. This can be seen by comparing the left and right panels of Figure 4B, which show the $\Delta = f(T)$ curves for $T_2 = 195$°C and 205°C, respectively. Increasing T_2 enables the melting of a larger fraction of Bi. Correspondingly, this leaves a larger fraction of undercooled Bi upon cooling down, which then translates into an increased hysteresis height. In line with the previously demonstrated analog phase tuning properties, we find that Δ_{23} can be finely tuned, as seen in Figure 4C. Therefore, the phase of the p-polarized reflected light can be tuned to the chosen value by heating the PCM to a selected temperature, and the phase value obtained remains stable when cooling down over a broad temperature range of about 100°C. This endows the PCM with analog optical memory capabilities.

2.4 Tentative performance benchmarking for potential applications

Based on these findings, we propose that the Bi-based PCMs are appealing candidates for thermally driven applications that require analog optical memory capabilities in the visible range, such as rewritable optical data storage platforms with enhanced information density or bistable photonic switches with a tunable "on" state. In this context, in order to compare the performance of Bi-based PCMs with those of other types of PCMs that can be tuned in an analog way (for instance VO_2-based PCMs and GST-based PCMs), we have realized a tentative benchmarking of their active optical phase tuning performance. This benchmarking, which is summarized in Table 1, considers the following aspects.

(i) The *optical phase tuning magnitude in the visible*. For an optimal device operation from an optical point of view, the magnitude of the optical phase tuning

Table 1: The tentative benchmarking of the active optical phase tuning performance of Bi-, VO_2- and GST-based PCMs for the thermally driven applications requiring analog optical memory capabilities in the visible range, such as rewritable optical data storage platforms with enhanced information density or bistable photonic switches with a tunable "on" state.

	Bi-based	VO_2-based	GST-based
Optical phase tuning magnitude	(+) Broad (+) Broadband	(+) Broad (–) Narrowband	(+) Broad (+) Broadband
Analog tuned state stability	(+) Good (semi-volatile[a])	(–) Low (volatile)	(++) Excellent (non-volatile)
Energy efficiency (write/store/erase)	(+) Write: heat <200°C (+) Store: bring Erase temp to room temperature? (++) Erase: cool	(++) Write: heat 65°C (–) Store: maintain 65°C (++) Erase: cool	(+) Write: heat 250°C (++) Store: no energy (– –) Erase: heat 600°C

[a]Wide hysteresis; This benchmarking considers three aspects: the optical phase tuning magnitude in the visible, the analog tuned state stability and the energy efficiency of operation (write/store/erase the analog tuned state).

allowed by the PCM must be as broad as possible, in an as broad spectral region as possible in the visible. In this context, the optical phase tuning magnitude of the Bi-based PCM considered in this work has been compared with that of the VO_2- and GST-based PCMs with the same structure by means of numerical simulations described in Appendix A. Upon the complete phase transition of the active material, the three PCMs considered in this study enable a tuning of the phase of visible light with a broad magnitude. However, the Bi- and GST-based ones present the advantage of enabling such tuning in a broader spectral region than the VO_2-based one. Therefore, from an optical point of view, the active phase tuning performance of the Bi-based PCM with the structure considered in this work is comparable to (resp. superior to) that of the GST-based PCM (resp. VO_2-based PCM) with the same structure.

(ii) The *stability of the analog tuned state* and *energy efficiency of the PCM operation*. For an optimal device operation from the point of view of reliability and energy consumption, the PCM should be brought to the analog tuned state ("write") with a moderate energy supply, it must remain stable in that state ("store") with no need for an energy supply, and it must be returned to its initial state ("erase") at a low energetic cost. In this regard, the ideal thermally driven PCM presents a wide hysteresis with a moderate upper temperature and with the initial state being recovered sharply very near room temperature upon cooling. The VO_2-based PCMs can be operated relatively close to room temperature (~65°C). However, their volatile phase transition shows a narrow hysteresis, so that continuous heating is needed to maintain the analog tuned state. GST-based PCMs are based on a non-volatile phase transition that enables the analog tuned state (reached near 250°C) to remain stable without heating. However, in the GST-based PCMs, returning to the initial state requires a high temperature heating (~600°C). In contrast with these materials, Bi-based PCMs are based on a semi-volatile phase transition that presents a wide hysteresis (~100°C width) and enables the recovery of the initial state upon cooling. The upper temperature and initial state recovery temperature of the hysteresis, which are ~200°C and ~90°C, respectively, could be decreased by building the Bi-based PCMs from smaller Bi nanostructures that undergo solidification closer to room temperature. This points at Bi-based PCMs as appealing candidates from the points of view of stability and energy efficiency, as they compare favorably with VO_2- and GST-based PCMs on these aspects.

3 Conclusions

In summary, we have reported that Bi-based PCMs enable the active and analog tuning of the phase of p-polarized reflected light at photon energies in the visible. The PCM is formed by a multilayer structure consisting of 2D assemblies of polydisperse Bi nanostructures embedded in a refractory and transparent Al_2O_3 matrix. This nanostructured metamaterial has been fully grown by pulsed laser deposition without the need for lithography techniques. Based on this PCM, we have demonstrated the analog phase tuning by heating to a suitably chosen temperature to melt a controlled fraction of the Bi nanostructures. In the current study, the maximum phase tuning of 320° (1.8 π) has been obtained at 230°C by fully melting all the Bi nanostructures. After cooling down to 25°C, the Bi nanostructures return to their initial solid state, thus

demonstrating the full reversibility of the PCM operation. We checked this reversibility during repeated experiments over a period of one year, and our results demonstrated the stability of the system. In addition, upon decreasing the temperature, the undercooling of the Bi nanostructures provides the PCM with a wide hysteretic response, which leaves the analog-tuned phase stable over a temperature range of about 100°C. This endows the PCM with analog optical memory capabilities.

Based on these findings, we propose that the Bi-based PCMs are appealing candidates for thermally driven applications that require analog optical memory capabilities in the visible range, such as rewritable optical data storage platforms with enhanced information density, or bistable photonic switches with a tunable "on" state. In the context of these applications, the Bi-based PCMs are an interesting alternative to the established PCMs (e.g. the VO_2- and GST-based PCMs) not only because of their excellent optical properties, but because they compare favorably with these other PCMs from the points of view of stability and energy efficiency.

4 Methods

4.1 PCM fabrication

The Bi-based PCMs were grown by alternate pulsed laser deposition from pure casted Bi and ceramic Al_2O_3 targets sputtered sequentially onto a Si substrate. The deposition was performed in vacuum ($\approx 10^{-6}$ mbar) using an ArF excimer laser at 193 nm with a pulse duration of 12 ns and 5 Hz repetition rate. The energy densities on the Al_2O_3 and Bi targets were 2 mJ cm^{-2} and 0.75 mJ cm^{-2}, considering the different energies needed to achieve ablation of the different targets. First, an amorphous Al_2O_3 layer was deposited on which the Bi nanostructures were subsequently grown by using 300 pulses on the target. Then a layer of amorphous Al_2O_3 was deposited again in order to cover and embed the Bi nanostructures. This deposition procedure was repeated four more times. The details about the growth mechanisms of the Bi nanostructures are given in [23].

4.2 PCM structure

Cross-section images of the PCM were obtained with a Tecnai F20 transmission electron microscope after performing the focused ion-beam lift-out and milling of a piece of PCM to electron transparency. According to the images, the PCM has the following layered structure: Roughness (2 nm)/Al_2O_3 (15 nm)/Bi:Al_2O_3 (7 nm)/[Al_2O_3 (18 nm)/Bi:Al_2O_3 (6 nm)]$_4$/Al_2O_3 (22 nm)/Si.

For the demonstration of the tuning of the phase of light, we designed such a structure to include several [Al_2O_3/Bi:Al_2O_3] bilayers for three reasons. The first reason is to provide the PCM with sufficient thickness (142 nm) and several internal interfaces to enable the destructive interference leading to cancelation of R_p. With a single bilayer structure [Al_2O_3 (18 nm)/Bi:Al_2O_3 (6 nm)]/Si, these conditions are not met. The second reason is that, in order to maximize the sensitivity of the optical phase to the presence of the Bi nanostructures, several [Al_2O_3/Bi:Al_2O_3] bilayers must be grown rather than a single one on a thick Al_2O_3 buffer layer (that would also allow cancelation of R_p while providing a weaker light-Bi interaction). Note that the five bilayer structure was not optimized. Hence it would be interesting to explore different multilayer structures to tune the AOI or photon energy of R_p cancelation or achieve a stronger sensitivity of the optical phase to the presence of Bi. Third, growing several bilayers with our deposition system is not more difficult than growing a single bilayer. This is because the whole deposition is performed in vacuum and operated by an automatized system featuring an in situ optical growth monitoring setup.

4.3 Size and shape distribution

To obtain information about the in-plane structure of the composite Bi:Al_2O_3 nanolayers, a sandwich Al_2O_3/Bi:Al_2O_3/Al_2O_3 structure was grown with the same nominal parameters as the PCM on carbon-coated mica substrates. After deposition, the film was floated in de-ionized water and deposited on a Cu grid for observation. Figure 5 shows a transmission electron microscopy plan-view image of the resulting material. The light continuous background corresponds to the Al_2O_3 matrix, and the dark areas correspond to the deposited Bi nanostructures. Electron diffraction analysis showed that the Bi is crystalline, whereas the Al_2O_3 is amorphous. In the image, the Bi nanostructures show a morphology characterized by polydisperse sizes and shapes with lengths in the range from ~10 nm to ~100 nm.

4.4 Temperature-dependent optical properties

The temperature-dependent optical properties (ellipsometry and reflectance) of the PCM were measured with

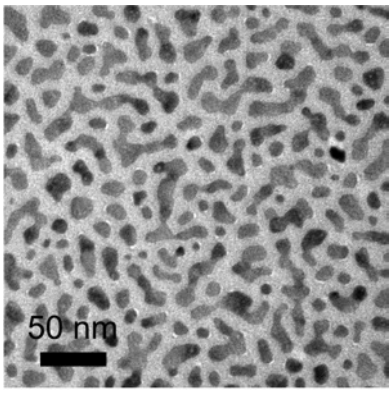

Figure 5: The plan view transmission electron microscopy image of a $Al_2O_3/Bi:Al_2O_3/Al_2O_3$ structure grown with the same nominal parameters as the PCM.

a Woollam VASE spectroscopic ellipsometer in a Polarizer/Retarder/Sample/Rotating Analyzer configuration and equipped with an Instec temperature control stage. During experiments in static conditions, we checked that the actual temperature of the PCM, which we measured with a thermocouple in contact with the sample surface, was equal to the one measured by the temperature control stage sensor.

To determine the effective dielectric function spectra of the composite nanolayers shown in Figure 2C, the spectra of the ellipsometric coefficients ψ and Δ were first measured for E between 1 eV and 3.5 eV with a 0.05 eV step at AOIs ranging from 25° to 75° with a 10° step. These measurements were done in static conditions at 25°C and 230°C. At each temperature, all the measured spectra were fitted simultaneously using a single multilayer model that mimicked the real layered structure as seen in the cross-section images. Fitting was done in the transfer matrix formalism, using the WVASE32 software (Woollam). The thicknesses of the composite and Al_2O_3 spacer layers were set and kept constant at the values measured from these images. The spectra of the dielectric functions of Al_2O_3 and Si were previously determined at each temperature from the ellipsometry measurements of an Al_2O_3 film grown on Si and of a bare Si substrate, respectively. The dielectric function of the nanocomposite layers was modeled as the sum of 11 Kramers-Kronig consistent Lorentz oscillators and a real offset. The amplitude, width and energy of these oscillators and the real offset were left free during the fit. An excellent fit quality was obtained at both temperatures (MSE <8). Such a large number of oscillators was used with the aim of reproducing very small/second order structures in the spectrum. However, using 4 and 3 oscillators is already enough to reproduce satisfactorily the first-order spectral features at 25°C and 230°C, respectively. The dielectric functions obtained with 11 oscillators and 3–4 oscillators are visually very similar. Therefore, the dielectric functions we provide are fully reliable, unique solutions. In addition, they are physically meaningful as their featureless spectra account for the observed broad size and shape distribution of the polydisperse Bi nanostructures. Note that, since we targeted an excellent fit quality, here we preferred to use oscillators instead of the available effective medium models that enable, at best, a good fit quality in the case of polydisperse systems (Bruggeman model). With the best fit dielectric functions, ψ and Δ were simulated as a function of E and AOI to draw the high-resolution maps shown in Figure 2D and E. This approach is equivalent to interpolating the experimental data measured at discrete E and AOIs.

The ψ and Δ spectra shown in Figure 3 were also measured under static conditions. The measurements at each temperature were done after heating the PCM from 25°C at a 2°C/min rate and waiting 10 min to ensure thermal stabilization. After measurement at each temperature, the PCM was cooled down at a rate of 2°C/min. The $\Delta = f(T)$ curves shown in Figure 4 were measured under dynamic conditions, i.e. Δ was continuously recorded while increasing and then decreasing the temperature at a rate of 2°C/min.

Acknowledgments: This research was supported by Spanish grants RTI2018-096498-B-I00, Funder Id: http://dx.doi.org/10.13039/100014440 (MCIU/AEI/FEDER, UE) and LINKA20044, Funder Id: http://dx.doi.org/10.13039/501100003339 (CSIC). AKPL is grateful to the National Science Foundation under Collaborative Grant #DMR 1600837, Funder Id: http://dx.doi.org/10.13039/100000001 for funding. Use of the Center for Nanoscale Materials, an Office of Science user facility, was supported by the U.S. Department of Energy, Office of Science, Office of Basic Energy Sciences, under Contract No. DE-AC02-06CH11357, Funder Id: http://dx.doi.org/10.13039/100006151. E.N.P. acknowledges funding from Comunidad de Madrid (Spain), Garantia Juvenil contract PEJ-2018-AI/IND-10888.

Appendix A

Comparison of the optical phase tuning magnitude of Bi-, VO_2- and GST- based PCMs

To compare the optical phase tuning magnitude of the Bi-based PCM considered in this work with those of

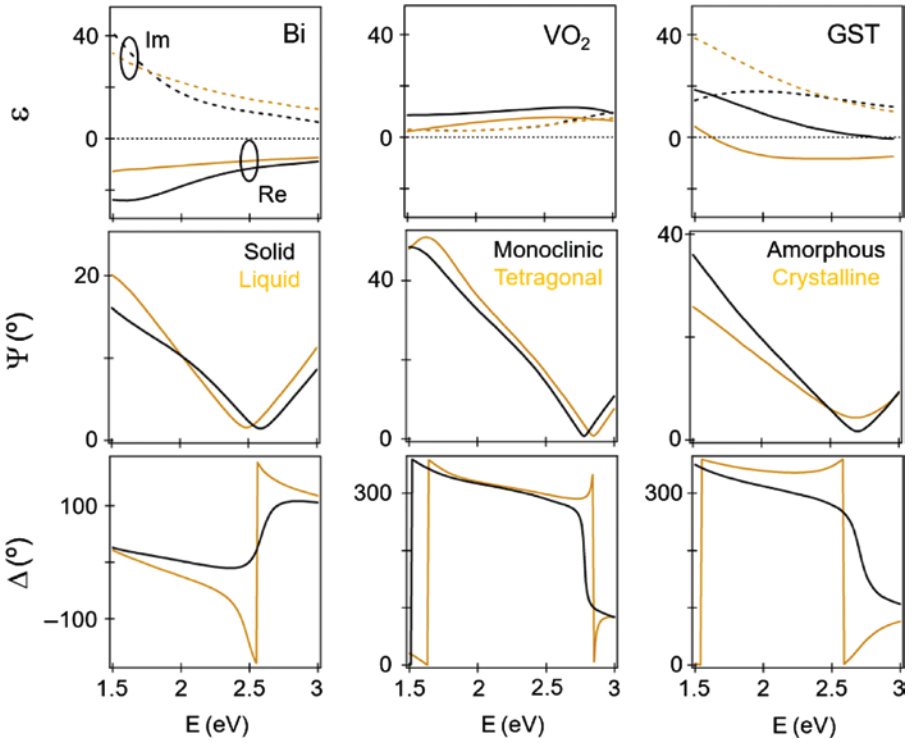

Figure 6: The simulated ψ and Δ spectra of Bi-, VO_2- and GST-based PCMs with the same layered structure as in Figure 2A, before/after the complete phase transition of the active material (black lines/orange lines) i.e. with solid/liquid Bi nanostructures, monoclinic/tetragonal VO_2 nanostructures and amorphous/crystalline GST nanostructures, respectively.
The simulations were done in the transfer matrix formalism (WVASE32 software). The three PCMs had the same layer thicknesses as those used for the ellipsometry analysis in Figure 2C. The composite nanolayers in the three PCMs (Bi:Al_2O_3, VO_2:Al_2O_3 and $Ge_2Sb_2Te_5$:Al_2O_3, respectively) were considered to present the same structure, and were thus modeled with the Bruggeman model with the same volume fraction (f = 37.6%) and depolarization factor (L = 0.48). These values were chosen because they enable the simulated ψ and Δ spectra of the Bi-based PCM to be in good qualitative agreement with the measured ones. The dielectric functions taken from the literature for Bi [25, 27], VO_2 [44] and $Ge_2Sb_2Te_5$ [45] are shown in the first row. The previously determined dielectric functions were used for Si and Al_2O_3. The simulated ψ and Δ spectra shown in the second and third rows have been taken at AOIs of 65.5°, 75° and 69.5°, respectively. These AOIs are those where the PCMs present a near-cancelation of ψ (R_p) in the visible range.

the VO_2- and GST-based PCMs with the same structure, numerical simulations of the ellipsometry spectra of these three types of PCMs were realized. As shown in Figure 6, the three PCMs display a near-cancelation of ψ (R_p) in the visible range, which translates to a Δ jump (located in the 2.6–2.7 eV region for the three PCMs). Around this jump, the phase of the reflected (p-polarized) light varies strongly upon the complete phase transition of the active material for the three PCMs (solid/liquid for Bi, monoclinic/tetragonal for VO_2, amorphous/crystalline for GST). Whereas this strong variation is restricted to a very narrow spectral region around the jump for the VO_2-based PCM, it occurs in a broader spectral region for the Bi-based and GST-based PCMs. In summary, the three PCMs considered can enable the active tuning of the phase of visible light with a broad magnitude, with the Bi- and GST-based PCMs presenting the advantage of enabling such tuning in a broader spectral region than the VO_2-based ones.

References

[1] Zheludev NI. Obtaining optical properties on demand. Science 2015;348:973–4.
[2] Shelton DJ, Coffey KR, Boreman DG. Experimental demonstration of tunable phase in thermochromic infrared-reflectarray metamaterial. Opt Express 2010;18:1330–5.
[3] Paik T, Hong S-H, Gaulding EA, et al. Solution-processed phase-change VO_2 metamaterials from colloidal vanadium oxide (VO_x) nanocrystals. ACS Nano 2014;8:798–806.
[4] Lei LY, Appavoo K, Ligmajer F, Sonnefraud Y, Haglund Jr. RF, Maier SA. Optically-triggered nanoscale memory effect in a hybrid plasmonic-phase changing nanostructure. ACS Photon 2015;2:1306–13.
[5] Shu FZ, Yu F-F, Peng R-W, et al. Dynamic plasmonic color generation based on phase transition vanadium dioxide. Adv Optical Mater 2018;6:1700939.
[6] Kim Y, Wu PC, Sokhoyan R, et al. Phase modulation with electrically tunable vanadium dioxide phase-change metasurfaces. Nano Lett 2019;19:3961–8.

[7] Vermeulen PA, Yimam DT, Loi MA, Kooi BJ. Multilevel reflectance switching of ultrathin phase-change films. J Appl Phys 2019;125:193105.
[8] Gholipour B, Zhang J, MacDonald KF, Hewak DW, Zheludev NI. An all-optical, non-volatile, bidirectional, phase-change meta-switch. Adv Mater 2013;25:3050–4.
[9] Chen YG, Kao TS, Ng B, et al. Hybrid phase-change plasmonic crystals for active tuning of lattice resonances. Opt Express 2013;21:13691–8.
[10] Hosseini P, Wright CD, Bhaskaran H. An optoelectronic framework enabled by low-dimensional phase-change films. Nature 2014;511:206–211.
[11] Chu CH, Tseng ML, Chen J, et al. Active dielectric metasurface based on phase-change medium. Laser Photonics Rev 2016;10:1600106.
[12] Li P, Yang X, Mass TWW, et al. Reversible optical switching of highly confined phonon-polaritons with an ultrathin phase-change material. Nature Mater 2016;15:870–6.
[13] Qu Y, Li Q, Du K, Cai L, Lu J, Qiu M. Dynamic thermal emission control based on ultrathin plasmonic metamaterials including phase-changing material GST. Laser Photonics Rev 2017;11:1700091.
[14] Hafermann M, Schöppe P, Rensberg J, Ronning C. Metasurfaces enabled by locally tailoring disorder in phase-change materials. ACS Photon 2018;5:5103–9.
[15] Ruiz de Galarreta C, Alexeev AM, Au Y-Y, et al. Nonvolatile reconfigurable phase-change metadevices for beam steering in the near infrared. Adv Funct Mater 2018;28:1704993.
[16] Meng Y, Behera JK, Wen S, et al. Ultrafast multilevel optical tuning with CSb_2Te_3 thin films. Adv Optical Mater 2018;6:1800360.
[17] Tian J, Luo H, Yang Y, et al. Active control of anapole states by structuring the phase-change alloy $Ge_2Sb_2Te_5$. Nature Commun 2019;10:396.
[18] Jafari M, Guo LJ, Rais-Zadeh M. A reconfigurable color reflector by selective phase change of GeTe in a multilayer structure. Adv Optical Mater 2019;7:1801214.
[19] Gholipour B, Piccinotti D, Karvounis A, MacDonald KF, Zheludev NI. Reconfigurable ultraviolet and high-energy visible dielectric metamaterials. Nano Lett 2019;19:1643–8.
[20] Jiménez de Castro M, Cabello F, Toudert J, Serna R, Haro-Poniatowski E. Potential of bismuth nanoparticles embedded in a glass matrix for spectral-selective thermo-optical devices. Appl Phys Lett 2014;105:113102.
[21] Toudert J. Spectroscopic ellipsometry for active nano- and meta- materials. Nanotechnol Rev 2014;3:223–45.
[22] Cuadrado A, Toudert J, Serna R. Polaritonic-to-plasmonic transition in optically-resonant bismuth nanospheres for high-contrast switchable ultraviolet meta-filters. IEEE Photonics J 2016;8:1–11.
[23] Toudert J, Serna R, Jimenez de Castro M. Exploring the optical potential of nano-bismuth: tunable plasmon resonances in the near ultraviolet-to-near infrared range. J Phys Chem. C 2012;116:20530–9.
[24] Toudert J, Serna R. Ultraviolet-visible interband plasmonics with p-block elements. Opt Mater Express 2016;6:2434–47.
[25] Toudert J, Serna R, Camps I, et al. Unveiling the far infrared-to-ultraviolet optical properties of bismuth for applications in plasmonics and nanophotonics. J Phys Chem C 2017;121:3511–21.
[26] Toudert J, Serna R. Interband transitions in semi-metals, semiconductors and topological insulators: a new driving force for plasmonics and nanophotonics. Opt Mater Express 2017;7:2299–325.
[27] Inagaki T, Arakawa ET, Cathers AR, Glastad KA. Optical properties of liquid Bi and Pb between 0.6 and 3.7 eV. Phys Rev B 1982;25:6130–68.
[28] Haro-Poniatowski E, Serna R, Jiménez de Castro M, Suárez-García A, Afonso CN, Vickridge I. Size-dependent thermo-optical properties of embedded Bi nanostructures. Nanotechnology 2008;19:485708.
[29] Toudert J, Wang X, Tallet C, Barois P, Aradian A, Ponsinet V. Plasmonic optical interferences for phase-monitored nanoscale sensing in low-loss three-dimensional metamaterials. ACS Photon 2015;2:1443–50.
[30] Ghobadi A, Hajian H, Butun B, Ozbay E. Strong light-matter interaction in lithography-free planar metamaterial perfect absorbers. ACS Photon 2018;5:4203–21.
[31] Ghobadi A, Hajian H, Gokbayrak M, Butun B, Ozbay E. Bismuth-based metamaterials: from narrowband reflective color filter to extremely broadband near perfect absorber. Nanophotonics 2019;8:823–32.
[32] Olson EA, Efremov MY, Zhang M, Zhang Z, Allen LH. Size-dependent melting of Bi nanoparticles. J Appl Phys 2005;97:034304.
[33] Kravets VG, Schedin F, Jalil R, et al. Singular phase nano-optics in plasmonic metamaterials for label-free single-molecule detection. Nature Mater 2013;12:304–9.
[34] Malassis L, Massé P, Tréguer-Delapierre M, et al. Topological darkness in self-assembled plasmonic metamaterials. Adv Mater 2013;26:324–30.
[35] Tsurimaki Y, Tong JK, Boriskin VN, et al. Topological engineering of interfacial optical Tamm states for highly sensitive near-singular-phase optical detection. ACS Photon 2018;5:929–38.
[36] Baraldi G, Garcia Pardo M, Gonzalo J, Serna R, Toudert J. Self-assembled nanostructured photonic-plasmonic metasurfaces for high-resolution optical thermometry. Adv Mater Interfaces 2018;5:1800241.
[37] Svedendahl M, Verre R, Käll M. Refractometric biosensing based on optical phase flips in sparse and short-range-ordered nanoplasmonic layers. Light Sci Appl 2014;3:e220.
[38] Park J, Kang J-H, Kim SJ, Liu X, Brongersma ML. Dynamic reflection phase and polarization control in metasurfaces. Nano Lett 2017;17:407–13.
[39] Jiang H, Reddy H, Shah D, et al. Modulating phase by metasurfaces with gated ultra-thin TiN films. Nanoscale 2019;11:11167–72.
[40] MacDonald KF, Fedotov VA, Pochon S, et al. Controlling the coexistence of structural phases and the optical properties of gallium nanoparticles with optical excitation. Eur Phys Lett 2004;67:614.
[41] Soares BF, MacDonald KF, Fedotov VA, Zheludev NI. Light-induced switching between structural forms with different optical properties in a single gallium nanoparticulate. Nano Lett 2005;5:2104–7.
[42] Knight MW, Coenen T, Yang Y, et al. Gallium plasmonics: deep subwavelength spectroscopic imaging of single and interacting gallium nanoparticles. ACS Nano 2015;9:2049–60.

[43] Gutiérrez Y, Losurdo M, García-Fernández P, et al. Gallium polymorphs: phase-dependent plasmonics. Adv Optical Mater 2019;7:1900307.
[44] Kana Kana JB, Ndjaka JM, Vignaud G, Gibaud A, Maaza M. Thermally tunable optical constants of vanadium dioxide thin films measured by spectroscopic ellipsometry. Opt Commun 2011;284:807–12.
[45] Shportko K, Kremers S, Woda M, Lencer D, Robertson J, Wuttig M. Resonant bonding in crystalline phase-change materials. Nature 2008;7:653–8.